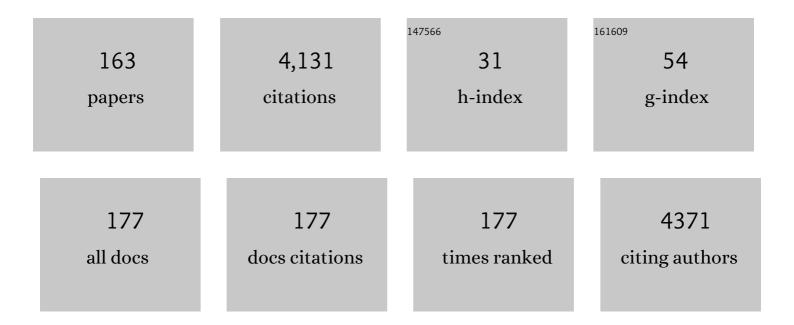
List of Publications by Year in descending order

Source: https://exaly.com/author-pdf/7023513/publications.pdf Version: 2024-02-01



**ΡΕΤΕΡ Β Νο**Δάμι

#	Article	IF	CITATIONS
1	Combined inhibition of BET family proteins and histone deacetylases as a potential epigenetics-based therapy for pancreatic ductal adenocarcinoma. Nature Medicine, 2015, 21, 1163-1171.	15.2	349
2	The evolution of image reconstruction for CT—from filtered back projection to artificial intelligence. European Radiology, 2019, 29, 2185-2195.	2.3	335
3	Initial Performance Characterization of a Clinical Noise–Suppressing Reconstruction Algorithm for MDCT. American Journal of Roentgenology, 2011, 197, 1404-1409.	1.0	138
4	Dual-energy CT: a phantom comparison of different platforms for abdominal imaging. European Radiology, 2018, 28, 2745-2755.	2.3	114
5	Spectral Photon-counting CT: Initial Experience with Dual–Contrast Agent K-Edge Colonography. Radiology, 2017, 283, 723-728.	3.6	111
6	In-vivo X-ray Dark-Field Chest Radiography of a Pig. Scientific Reports, 2017, 7, 4807.	1.6	83
7	Dual-layer spectral computed tomography: Virtual non-contrast in comparison to true non-contrast images. European Journal of Radiology, 2018, 104, 108-114.	1.2	83
8	Experimental feasibility of spectral photon-counting computed tomography with two contrast agents for the detection of endoleaks following endovascular aortic repair. European Radiology, 2018, 28, 3318-3325.	2.3	79
9	X-ray dark-field imaging of the human lung—A feasibility study on a deceased body. PLoS ONE, 2018, 13, e0204565.	1.1	76
10	Nanoparticle contrast agents for Xâ€ray imaging applications. Wiley Interdisciplinary Reviews: Nanomedicine and Nanobiotechnology, 2020, 12, e1642.	3.3	69
11	Assessment of quantification accuracy and image quality of a fullâ€body dualâ€layer spectral <scp>CT</scp> system. Journal of Applied Clinical Medical Physics, 2018, 19, 204-217.	0.8	65
12	Spectral photon-counting CT in cardiovascular imaging. Journal of Cardiovascular Computed Tomography, 2021, 15, 218-225.	0.7	65
13	GPU-based cone beam computed tomography. Computer Methods and Programs in Biomedicine, 2010, 98, 271-277.	2.6	63
14	Joint Statistical Iterative Material Image Reconstruction for Spectral Computed Tomography Using a Semi-Empirical Forward Model. IEEE Transactions on Medical Imaging, 2018, 37, 68-80.	5.4	63
15	Does Iterative Reconstruction Lower CT Radiation Dose: Evaluation of 15,000 Examinations. PLoS ONE, 2013, 8, e81141.	1.1	63
16	Simultaneous dual-contrast multi-phase liver imaging using spectral photon-counting computed tomography: a proof-of-concept study. European Radiology Experimental, 2017, 1, 25.	1.7	61
17	Spectral Photon-Counting Computed Tomography (SPCCT): in-vivo single-acquisition multi-phase liver imaging with a dual contrast agent protocol. Scientific Reports, 2019, 9, 8458.	1.6	56
18	Technical background of a novel detector-based approach to dual-energy computed tomography. Diagnostic and Interventional Radiology, 2020, 26, 68-71.	0.7	54

#	Article	IF	CITATIONS
19	Accuracy of iodine quantification in dual-layer spectral CT: Influence of iterative reconstruction, patient habitus and tube parameters. European Journal of Radiology, 2018, 102, 83-88.	1.2	53
20	Evaluation of a preclinical photon-counting CT prototype for pulmonary imaging. Scientific Reports, 2018, 8, 17386.	1.6	53
21	Is multidetector CT-based bone mineral density and quantitative bone microstructure assessment at the spine still feasible using ultra-low tube current and sparse sampling?. European Radiology, 2017, 27, 5261-5271.	2.3	47
22	Bone mineral density measurements derived from dual-layer spectral CT enable opportunistic screening for osteoporosis. European Radiology, 2019, 29, 6355-6363.	2.3	46
23	Synovitis in Patients with Early Inflammatory Arthritis Monitored with Quantitative Analysis of Dynamic Contrast-enhanced Optical Imaging and MR Imaging. Radiology, 2014, 270, 176-185.	3.6	45
24	Detection of synovitis in the hands of patients with rheumatologic disorders: Diagnostic performance of optical imaging in comparison with magnetic resonance imaging. Arthritis and Rheumatism, 2012, 64, 2489-2498.	6.7	44
25	Statistical iterative reconstruction algorithm for X-ray phase-contrast CT. Scientific Reports, 2015, 5, 10452.	1.6	43
26	Ultra Low Dose CT Pulmonary Angiography with Iterative Reconstruction. PLoS ONE, 2016, 11, e0162716.	1.1	42
27	Large field-of-view tiled grating structures for X-ray phase-contrast imaging. Review of Scientific Instruments, 2017, 88, 015104.	0.6	38
28	Non-invasive Differentiation of Kidney Stone Types using X-ray Dark-Field Radiography. Scientific Reports, 2015, 5, 9527.	1.6	37
29	Quantitative imaging using high-energy X-ray phase-contrast CT with a 70 kVp polychromatic X-ray spectrum. Optics Express, 2015, 23, 523.	1.7	35
30	Simultaneous wood and metal particle detection on dark-field radiography. European Radiology Experimental, 2018, 2, 1.	1.7	35
31	Reduction of Metal Artifact in Single Photon-Counting Computed Tomography by Spectral-Driven Iterative Reconstruction Technique. PLoS ONE, 2015, 10, e0124831.	1.1	33
32	Object Specific Trajectory Optimization for Industrial X-ray Computed Tomography. Scientific Reports, 2016, 6, 19135.	1.6	32
33	Bone mineral density measurements in vertebral specimens and phantoms using dual-layer spectral computed tomography. Scientific Reports, 2017, 7, 17519.	1.6	32
34	Evaluation of MR-derived CT-like images and simulated radiographs compared to conventional radiography in patients with benign and malignant bone tumors. European Radiology, 2019, 29, 13-21.	2.3	32
35	Imaging Liver Lesions Using Grating-Based Phase-Contrast Computed Tomography with Bi-Lateral Filter Post-Processing. PLoS ONE, 2014, 9, e83369.	1.1	31
36	Automatic detection of osteoporotic vertebral fractures in routine thoracic and abdominal MDCT. European Radiology, 2014, 24, 872-880.	2.3	31

#	Article	IF	CITATIONS
37	In-Vivo Assessment of Femoral Bone Strength Using Finite Element Analysis (FEA) Based on Routine MDCT Imaging: A Preliminary Study on Patients with Vertebral Fractures. PLoS ONE, 2015, 10, e0116907.	1.1	31
38	Depiction of pneumothoraces in a large animal model using x-ray dark-field radiography. Scientific Reports, 2018, 8, 2602.	1.6	31
39	Grating-based phase-contrast and dark-field computed tomography: a single-shot method. Scientific Reports, 2017, 7, 7476.	1.6	30
40	Direct quantitative material decomposition employing grating-based X-ray phase-contrast CT. Scientific Reports, 2018, 8, 16394.	1.6	30
41	Correlation of X-Ray Vector Radiography to Bone Micro-Architecture. Scientific Reports, 2014, 4, 3695.	1.6	29
42	Penalized maximum likelihood reconstruction for x-ray differential phase-contrast tomography. Medical Physics, 2015, 43, 188-194.	1.6	28
43	Accuracy of Calcium Scoring calculated from contrast-enhanced Coronary Computed Tomography Angiography using a dual-layer spectral CT: A comparison of Calcium Scoring from real and virtual non-contrast data. PLoS ONE, 2018, 13, e0208588.	1.1	28
44	Trabecular bone anisotropy imaging with a compact laser-undulator synchrotron x-ray source. Scientific Reports, 2017, 7, 14477.	1.6	26
45	Differentiation between blood and iodine in a bovine brain—Initial experience with Spectral Photon-Counting Computed Tomography (SPCCT). PLoS ONE, 2019, 14, e0212679.	1.1	26
46	Validation of a Low Dose Simulation Technique for Computed Tomography Images. PLoS ONE, 2014, 9, e107843.	1.1	25
47	Phase-Contrast Hounsfield Units of Fixated and Non-Fixated Soft-Tissue Samples. PLoS ONE, 2015, 10, e0137016.	1.1	25
48	Generalized ComBat harmonization methods for radiomic features with multi-modal distributions and multiple batch effects. Scientific Reports, 2022, 12, 4493.	1.6	25
49	Threeâ€dimensional printing of patientâ€specific lung phantoms for CT imaging: Emulating lung tissue with accurate attenuation profiles and textures. Medical Physics, 2022, 49, 825-835.	1.6	25
50	Coherent Superposition in Grating-Based Directional Dark-Field Imaging. PLoS ONE, 2013, 8, e61268.	1.1	24
51	EVALUATION OF DOSE REDUCTION POTENTIALS OF A NOVEL SCATTER CORRECTION SOFTWARE FOR BEDSIDE CHEST X-RAY IMAGING. Radiation Protection Dosimetry, 2016, 169, 60-67.	0.4	24
52	Multidetector Computed Tomography Imaging. Journal of Computer Assisted Tomography, 2018, 42, 441-447.	0.5	24
53	Analysis and correction of bias induced by phase stepping jitter in grating-based X-ray phase-contrast imaging. Optics Express, 2018, 26, 12707.	1.7	23
54	Liquid Embolic Agents in Spectral X-Ray Photon-Counting Computed Tomography using Tantalum K-Edge Imaging. Scientific Reports, 2019, 9, 5268.	1.6	23

#	Article	IF	CITATIONS
55	Imaging of Hsp70-positive tumors with cmHsp70.1 antibody-conjugated gold nanoparticles. International Journal of Nanomedicine, 2015, 10, 5687.	3.3	22
56	Filtered region of interest coneâ€beam rotational angiography. Medical Physics, 2010, 37, 694-703.	1.6	21
57	Cardioprotective C-kit+ Bone Marrow Cells Attenuate Apoptosis after Acute Myocardial Infarction in Mice - In-vivo Assessment with Fluorescence Molecular Imaging. Theranostics, 2013, 3, 903-913.	4.6	21
58	Dual-layer spectral computed tomography: measuring relative electron density. European Radiology Experimental, 2018, 2, 20.	1.7	21
59	Three-material decomposition with dual-layer spectral CT compared to MRI for the detection of bone marrow edema in patients with acute vertebral fractures. Skeletal Radiology, 2018, 47, 1533-1540.	1.2	21
60	Imaging features in post-mortem x-ray dark-field chest radiographs and correlation with conventional x-ray and CT. European Radiology Experimental, 2019, 3, 25.	1.7	21
61	Multi-detector CT imaging: impact of virtual tube current reduction and sparse sampling on detection of vertebral fractures. European Radiology, 2019, 29, 3606-3616.	2.3	21
62	Evaluation of guidewire path reproducibility. Medical Physics, 2008, 35, 1884-1892.	1.6	20
63	Effects of dose reduction on bone strength prediction using finite element analysis. Scientific Reports, 2016, 6, 38441.	1.6	20
64	Radioprotective Garment-Inspired Biodegradable Polymetal Nanoparticles for Enhanced CT Contrast Production. Chemistry of Materials, 2020, 32, 381-391.	3.2	20
65	First-generation clinical dual-source photon-counting CT: ultra-low-dose quantitative spectral imaging. European Radiology, 2022, 32, 8579-8587.	2.3	20
66	CT pulmonary angiography: dose reduction via a next generation iterative reconstruction algorithm. Acta Radiologica, 2019, 60, 478-487.	0.5	19
67	Joint learning of ultrasonic backscattering statistical physics and signal confidence primal for characterizing atherosclerotic plaques using intravascular ultrasound. Medical Image Analysis, 2014, 18, 103-117.	7.0	18
68	Improved detection rates and treatment planning of head and neck cancer using dual-layer spectral CT. European Radiology, 2018, 28, 4925-4931.	2.3	18
69	Dual layer computed tomography: Reduction of metal artefacts from posterior spinal fusion using virtual monoenergetic imaging. European Journal of Radiology, 2018, 105, 195-203.	1.2	18
70	DXA-equivalent quantification of bone mineral density using dual-layer spectral CT scout scans. European Radiology, 2019, 29, 4624-4634.	2.3	18
71	Dynamic CT Perfusion Imaging of the Myocardium: A Technical Note on Improvement of Image Quality. PLoS ONE, 2013, 8, e75263.	1.1	18
72	Evaluation of an iterative model–based reconstruction algorithm for low-tube-voltage (80ÂkVp) computed tomography angiography. Journal of Medical Imaging, 2014, 1, 033501.	0.8	17

#	Article	IF	CITATIONS
73	<scp>CNN</scp> as model observer in a liver lesion detection task for xâ€ray computed tomography: A phantom study. Medical Physics, 2018, 45, 4439-4447.	1.6	17
74	Quantitative Three-Dimensional Imaging of Lipid, Protein, and Water Contents via X-Ray Phase-Contrast Tomography. PLoS ONE, 2016, 11, e0151889.	1.1	17
75	Evaluation of an iterative model-based CT reconstruction algorithm by intra-patient comparison of standard and ultra-low-dose examinations. Acta Radiologica, 2018, 59, 1225-1231.	0.5	16
76	Spectral Angiography Material Decomposition Using an Empirical Forward Model and a Dictionary-Based Regularization. IEEE Transactions on Medical Imaging, 2018, 37, 2298-2309.	5.4	16
77	Acute infarction after mechanical thrombectomy is better delineable in virtual non-contrast compared to conventional images using a dual-layer spectral CT. Scientific Reports, 2018, 8, 9329.	1.6	16
78	MRI-derived porosity index is associated with whole-bone stiffness and mineral density in human cadaveric femora. Bone, 2021, 143, 115774.	1.4	16
79	Planning image-guided endovascular interventions: guidewire simulation using shortest path algorithms. , 2007, , .		15
80	Simulated Cystic Renal Lesions: Quantitative X-ray Phase-Contrast CT—An in Vitro Phantom Study. Radiology, 2014, 272, 739-748.	3.6	15
81	Quantitative dual-energy micro-CT with a photon-counting detector for material science and non-destructive testing. PLoS ONE, 2019, 14, e0219659.	1.1	15
82	Liver lesion localisation and classification with convolutional neural networks: a comparison between conventional and spectral computed tomography. Biomedical Physics and Engineering Express, 2020, 6, 015038.	0.6	15
83	Opportunistic osteoporosis screening: contrast-enhanced dual-layer spectral CT provides accurate measurements of vertebral bone mineral density. European Radiology, 2021, 31, 3147-3155.	2.3	15
84	Coronary CT angiography in step-and-shoot technique with 256-slice CT: Impact of the field of view on image quality, craniocaudal coverage, and radiation exposure. European Journal of Radiology, 2012, 81, 1562-1568.	1.2	14
85	Real-time endovascular guidewire position simulation using shortest path algorithms. International Journal of Computer Assisted Radiology and Surgery, 2009, 4, 597-608.	1.7	13
86	Evaluation of the potential of phase-contrast computed tomography for improved visualization of cancerous human liver tissue. Zeitschrift Fur Medizinische Physik, 2013, 23, 204-211.	0.6	13
87	X-ray Dark-Field Vector Radiography—A Novel Technique for Osteoporosis Imaging. Journal of Computer Assisted Tomography, 2015, 39, 286-289.	0.5	13
88	Xâ€ <b>ғ</b> ay computed tomography using curvelet sparse regularization. Medical Physics, 2015, 42, 1555-1565.	1.6	13
89	Combining radiomic phenotypes of non-small cell lung cancer with liquid biopsy data may improve prediction of response to EGFR inhibitors. Scientific Reports, 2021, 11, 9984.	1.6	13

90 A versatile tomographic forward- and back-projection approach on multi-GPUs. , 2014, , .

12

#	Article	IF	CITATIONS
91	Nonlinear statistical iterative reconstruction for propagation-based phase-contrast tomography. APL Bioengineering, 2018, 2, 016105.	3.3	12
92	Hunting for necrosis in the shadows of intravascular ultrasound. Computerized Medical Imaging and Graphics, 2014, 38, 104-112.	3.5	11
93	A post-processing algorithm for spectral CT material selective images using learned dictionaries. Biomedical Physics and Engineering Express, 2017, 3, 025009.	0.6	11
94	MDCT-based Finite Element Analysis of Vertebral Fracture Risk: What Dose is Needed?. Clinical Neuroradiology, 2019, 29, 645-651.	1.0	11
95	Low-dose and sparse sampling MDCT-based femoral bone strength prediction using finite element analysis. Archives of Osteoporosis, 2020, 15, 17.	1.0	11
96	Predicting Vertebral Bone Strength Using Finite Element Analysis for Opportunistic Osteoporosis Screening in Routine Multidetector Computed Tomography Scans—A Feasibility Study. Frontiers in Endocrinology, 2020, 11, 526332.	1.5	11
97	Prediction of Vertebral Failure Load by Using X-Ray Vector Radiographic Imaging. Radiology, 2015, 275, 553-561.	3.6	10
98	X-ray deconvolution microscopy. Biomedical Optics Express, 2016, 7, 1227.	1.5	10
99	Spectral Computed Tomography Angiography With a Gadolinium-based Contrast Agent. Journal of Thoracic Imaging, 2018, 33, 246-253.	0.8	10
100	CTPA with a conventional CT at 100 kVp vs. a spectral-detector CT at 120 kVp: Comparison of radiation exposure, diagnostic performance and image quality. European Journal of Radiology Open, 2020, 7, 100234.	0.7	10
101	In-vivo X-ray dark-field computed tomography for the detection of radiation-induced lung damage in mice. Physics and Imaging in Radiation Oncology, 2021, 20, 11-16.	1.2	10
102	Optimizing radiation exposure for CT localizer radiographs. Zeitschrift Fur Medizinische Physik, 2017, 27, 145-158.	0.6	9
103	Effect of radiation dose reduction on texture measures of trabecular bone microstructure: an in vitro study. Journal of Bone and Mineral Metabolism, 2018, 36, 323-335.	1.3	9
104	3D grating-based X-ray phase-contrast computed tomography for high-resolution quantitative assessment of cartilage: An experimental feasibility study with 3T MRI, 7T MRI and biomechanical correlation. PLoS ONE, 2019, 14, e0212106.	1.1	9
105	Assessment of femoral neck bone metabolism using 18F-sodium fluoride PET/CT imaging. Bone, 2020, 136, 115351.	1.4	9
106	Dosimetry on first clinical darkâ€field chest radiography. Medical Physics, 2021, 48, 6152-6159.	1.6	9
107	Wound ballistic evaluation of the TASER® XREP ammunition. International Journal of Legal Medicine, 2013, 127, 119-126.	1.2	8
108	Effect of Low-Dose MDCT and Iterative Reconstruction on Trabecular Bone Microstructure Assessment. PLoS ONE, 2016, 11, e0159903.	1.1	8

#	Article	IF	CITATIONS
109	Advanced Non-Destructive Ocular Visualization Methods by Improved X-Ray Imaging Techniques. PLoS ONE, 2017, 12, e0170633.	1.1	8
110	Perfusion-ventilation CT via three-material differentiation in dual-layer CT: a feasibility study. Scientific Reports, 2019, 9, 5837.	1.6	8
111	A comparison of material decomposition techniques for dual-energy CT colonography. Proceedings of SPIE, 2015, 9412, .	0.8	7
112	A Monte Carlo software bench for simulation of spectral k-edge CT imaging: Initial results. Physica Medica, 2015, 31, 398-405.	0.4	7
113	Dose reduction in abdominal CT: The road to submillisievert imaging. European Radiology, 2018, 28, 2743-2744.	2.3	7
114	Finite Element Analysis-Based Vertebral Bone Strength Prediction Using MDCT Data: How Low Can We Go?. Frontiers in Endocrinology, 2020, 11, 442.	1.5	7
115	Radiomic Phenotypes for Improving Early Prediction of Survival in Stage III Non-Small Cell Lung Cancer Adenocarcinoma after Chemoradiation. Cancers, 2022, 14, 700.	1.7	7
116	PixelPrint: three-dimensional printing of realistic patient-specific lung phantoms for CT imaging. , 2022, , .		7
117	Optimization of three-dimensional angiographic data obtained by self-calibration of multiview imaging. Medical Physics, 2006, 33, 3901-3911.	1.6	6
118	Dictionary-based image denoising for dual energy computed tomography. Proceedings of SPIE, 2016, , .	0.8	6
119	Effect of Statistically Iterative Image Reconstruction on Vertebral Bone Strength Prediction Using Bone Mineral Density and Finite Element Modeling. Journal of Computer Assisted Tomography, 2019, 43, 61-65.	0.5	6
120	Systematic Evaluation of Low-dose MDCT for Planning Purposes of Lumbosacral Periradicular Infiltrations. Clinical Neuroradiology, 2020, 30, 749-759.	1.0	6
121	Grating-based phase-contrast CT (PCCT): histopathological correlation of human liver cirrhosis and hepatocellular carcinoma specimen. Journal of Clinical Pathology, 2020, 73, 483-487.	1.0	6
122	Low-dose MDCT: evaluation of the impact of systematic tube current reduction and sparse sampling on the detection of degenerative spine diseases. European Radiology, 2021, 31, 2590-2600.	2.3	6
123	Spectral CT quantification stability and accuracy for pediatric patients: A phantom study. Journal of Applied Clinical Medical Physics, 2021, 22, 16-26.	0.8	6
124	Potential of dual-layer spectral CT for the differentiation between hemorrhage and iodinated contrast medium in the brain after endovascular treatment of ischemic stroke patients. Clinical Imaging, 2021, 79, 158-164.	0.8	6
125	3D reconstruction of the carotid artery from two views using a single centerline. International Congress Series, 2004, 1268, 177-182.	0.2	5
126	Regularized iterative integration combined with non-linear diffusion filtering for phase-contrast x-ray computed tomography. Optics Express, 2014, 22, 32107.	1.7	5

#	Article	IF	CITATIONS
127	Metric-guided regularisation parameter selection for statistical iterative reconstruction in computed tomography. Scientific Reports, 2019, 9, 6016.	1.6	5
128	Low-Dose MDCT of Patients With Spinal Instrumentation Using Sparse Sampling: Impact on Metal Artifacts. American Journal of Roentgenology, 2021, 216, 1308-1317.	1.0	5
129	Impact of dose reduction and iterative model reconstruction on multi-detector CT imaging of the brain in patients with suspected ischemic stroke. Scientific Reports, 2021, 11, 22271.	1.6	5
130	Evaluation of a method for improving the detection of hepatocellular carcinoma. European Radiology, 2014, 24, 250-255.	2.3	4
131	Dynamic CT perfusion imaging of the myocardium using a wide-detector scanner: a semiquantitative analysis in an animal model. Clinical Imaging, 2014, 38, 675-680.	0.8	4
132	CT Angiography. Academic Radiology, 2017, 24, 131-136.	1.3	4
133	Revising the lower statistical limit of x-ray grating-based phase-contrast computed tomography. PLoS ONE, 2017, 12, e0184217.	1.1	4
134	Tilted grating phase-contrast computed tomography using statistical iterative reconstruction. Scientific Reports, 2018, 8, 6608.	1.6	4
135	Tube Current Reduction in CT Angiography: How Low Can We Go in Imaging of Patients With Suspected Acute Stroke?. American Journal of Roentgenology, 2019, 213, 410-416.	1.0	4
136	Spectral-detector based x-ray absorptiometry (SDXA): in-vivo bone mineral density measurements in patients with and without osteoporotic fractures. Biomedical Physics and Engineering Express, 2020, 6, 055021.	0.6	4
137	Preliminary clinical results: an analyzing tool for 2D optical imaging in detection of active inflammation in rheumatoid arthritis. Proceedings of SPIE, 2011, , .	0.8	3
138	Quantitative positron emission tomography imaging in the presence of iodinated contrast media using electron density quantifications from dualâ€energy computed tomography. Medical Physics, 2021, 48, 273-286.	1.6	3
139	Quantitative analysis of speckle-based X-ray dark-field imaging using numerical wave-optics simulations. Scientific Reports, 2021, 11, 16113.	1.6	3
140	Diagnostic value of sparse sampling computed tomography for radiation dose reduction: initial results. , 2018, , .		3
141	Combining spectral CT acquisition methods for high-sensitivity material decomposition. , 2020, 11312, .		3
142	Registration of vascular 3D data sets obtained from multiple-view reconstructions. International Congress Series, 2004, 1268, 329-334.	0.2	2
143	Generating of 3D data during neurovascular interventions by using multi-projection imaging. International Congress Series, 2005, 1281, 334-338.	0.2	2

144 Toward region of interest computer tomography. , 2009, , .

#	Article	IF	CITATIONS
145	A method for improving iodine contrast enhancement in abdominal computed tomography: experimental study in a pig model. European Radiology, 2013, 23, 985-990.	2.3	2
146	X-ray vector radiography of a human hand. , 2017, , .		2
147	Ex vivo characterization of pathologic fluids with quantitative phase-contrast computed tomography. European Journal of Radiology, 2017, 86, 99-104.	1.2	2
148	Sparse sampling computed tomography (SpSCT) for detection of pulmonary embolism: a feasibility study. European Radiology, 2019, 29, 5950-5960.	2.3	2
149	Towards subject-level cerebral infarction classification of CT scans using convolutional networks. PLoS ONE, 2020, 15, e0235765.	1.1	2
150	Quantitative imaging of the spine in adolescent idiopathic scoliosis: shifting the paradigm from diagnostic to comprehensive prognostic evaluation. European Journal of Orthopaedic Surgery and Traumatology, 2021, 31, 1273-1285.	0.6	2
151	Spectral CT using a fine grid structure and varying xâ€ray incidence angle. Medical Physics, 2021, 48, 6412-6420.	1.6	2
152	Sparse-sampling computed tomography for detection of endoleak after endovascular aortic repair (EVAR). European Journal of Radiology, 2021, 142, 109843.	1.2	2
153	Region of interest processing for iterative reconstruction in x-ray computed tomography. , 2015, , .		1
154	Low-Dose Dual KVP Switching Using A Static Coded Aperture. , 2021, , .		1
155	Evaluation of a machine learning based model observer for x-ray CT. , 2018, , .		1
156	Grating-based Spectral CT using Small Angle X-ray Beam Deflections. , 2020, 2020, 630-633.		1
157	Hepatic dual-contrast CT imaging: slow triple kVp switching CT with CNN-based sinogram completion and material decomposition. Journal of Medical Imaging, 2022, 9, 014003.	0.8	1
158	Clinical evaluation of angiographic multiple-view 3D reconstruction. International Journal of Computer Assisted Radiology and Surgery, 2009, 4, 497-508.	1.7	0
159	Rapid dynamic radial MRI via reference image enforced histogram constrained reconstruction. Journal of Magnetic Resonance, 2014, 240, 1-7.	1.2	0
160	Effect of low-dose CT and iterative reconstruction on trabecular bone microstructure assessment. Proceedings of SPIE, 2016, , .	0.8	0
161	Low-dose MDCT: evaluation of the impact of systematic tube current reduction and sparse sampling on quantitative paraspinal muscle assessment. Quantitative Imaging in Medicine and Surgery, 2021, 11, 3042-3050.	1.1	0
162	Low-Dose Simulation and Sparse Sampling with Statistical Iterative Reconstruction: Dose Reduction in MDCT-Based Bone Mineral Density and Microstructure Assessment. Seminars in Musculoskeletal Radiology, 2017, 21, S1-S5.	0.4	0

#	Article	IF	CITATIONS
163	Sparse-sampling computed tomography for pulmonary imaging. , 2019, , .		0